Letter

Manipulating the Injected Energy Flux via Host-Sensitized Nanostructure for Improving Multiphoton Upconversion Luminescence of Tm^{3+}

Xiaoyu Xie, Qiqing Li, Haoran Chen, Wang Wang, Fengxia Wu, Langping Tu, Youlin Zhang, Xianggui Kong, and Yulei Chang*

Read Online

ACCESS | Metrics & More | Article Recommendations | Supporting Information

ABSTRACT: Combating the concentration quenching effect by increasing the concentration of sensitized rare-earth ions in rational design upconversion nanostructure will make it easier to utilize injection energy flux and transfer it to emitters, resulting in improved upconversion luminescence (UCL). We proposed a host-sensitized nanostructure (active core@luminescent shell@inert shell) to improve multiphoton UCL of Tm^{3+} based on the LiLnF$_4$ host. Yb^{3+} ions were isolated in the core as energy absorbents, and Tm^{3+} was doped in the interior LiYbF$_4$ host shell. Compared with sandwich structured nanocrystals (Y@Y:Yb/Tm@Y), reverse structure (YbTm@Yb@Y), and fully doped structure (YbTm@YbTm@Y), the proposed structure achieved the highest efficiency of multiphoton UCL and favored a better FRET-based application performance as the Tm^{3+} located at an optimized spatial distribution. Furthermore, steady-state and dynamic analysis results demonstrate that by manipulating the spatial distribution of the active ions, excited energy can be tuned to enable multiphoton upconversion enhancement, overcoming the conventional limitations.

KEYWORDS: multiphoton upconversion, energy migration, FRET, concentration quenching
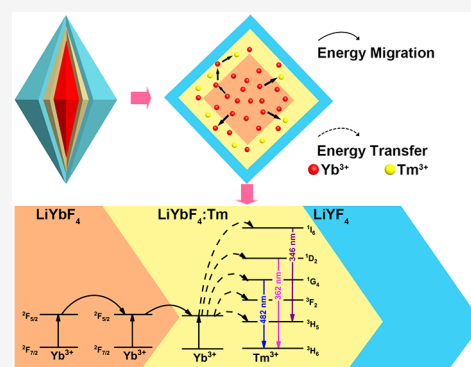
Lanthanide-doped upconversion nanoparticles (UCNPs), which can convert two or more low-energy pump photons into one high-energy output photon, allow for the emission of a wide range of wavelengths from near-infrared (NIR) to ultraviolet (UV). Emissions from Tm^{3+}-based UCNPs, typically Yb/Tm co-doping, generate UV/blue emission with a large anti-Stokes shift, essential in biomedicine,[1−4] photocatalysis,[5−8] etc. However, many detrimental factors, such as concentration quenching, cross-relaxation, and surface quenching, continue to limit the brightness and multiphoton emission efficiency of these UCNPs. Significantly, at high-lying emission levels, the complex multiphoton transition process of Tm^{3+} easily renders excited energy consumption. Improving Tm^{3+} multiphoton emission is critical to increasing energy injection while minimizing excited-state energy dissipation via unfavorable energy transport pathways.

Although increasing the concentration of the dopants appears to be the simplest way to improve the absorption cross-section for energy harvesting, concentration quenching restricts the doping level of sensitizer and activator ions.[9−11] Recent research has focused on elucidating the concentrating effects in heavily doped UCNPs such as NaErF$_4$@NaYF$_4$, NaYbF$_4$, and NaErF$_4$@NaYF$_4$@NaYbF$_4$:0.5% Tm@NaYF$_4$ to improve UCL brightness.[12−15] Furthermore, the upconversion processes of activators such as lifetime, intensity, and transition

selectivity can be tuned by spatially partitioned doping of Yb^{3+} or Yb^{3+}/Nd^{3+} ions (i.e., independent sensitized shells to avoid cross-talk).[16,17] The introduction of Nd^{3+} as the sensitizer ions could modulate the excitation wavelength to 808 nm through Nd^{3+} → Yb^{3+} energy transfer (ET).[18] Moreover, several studies on Yb-based fluoride host materials revealed that this host could positively influence upconversion emission. Besides, the Yb^{3+} could take full advantage of the 980 nm energy flux for their larger absorption cross-section. Conversely, the high level of Yb^{3+} content could mediate an efficient long-range energy migration/transfer to excite activator ions due to its single excited energy level.[19] However, introducing a high concentration of active ions does not contribute to the same degree of luminescence enhancement as increasing concentration due to excited-state energy dissipation caused by adverse energy transport, such as defects, cross-talk, reverse ET.[20] As a result, a rational structural design is significant for energy manipulation
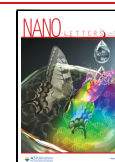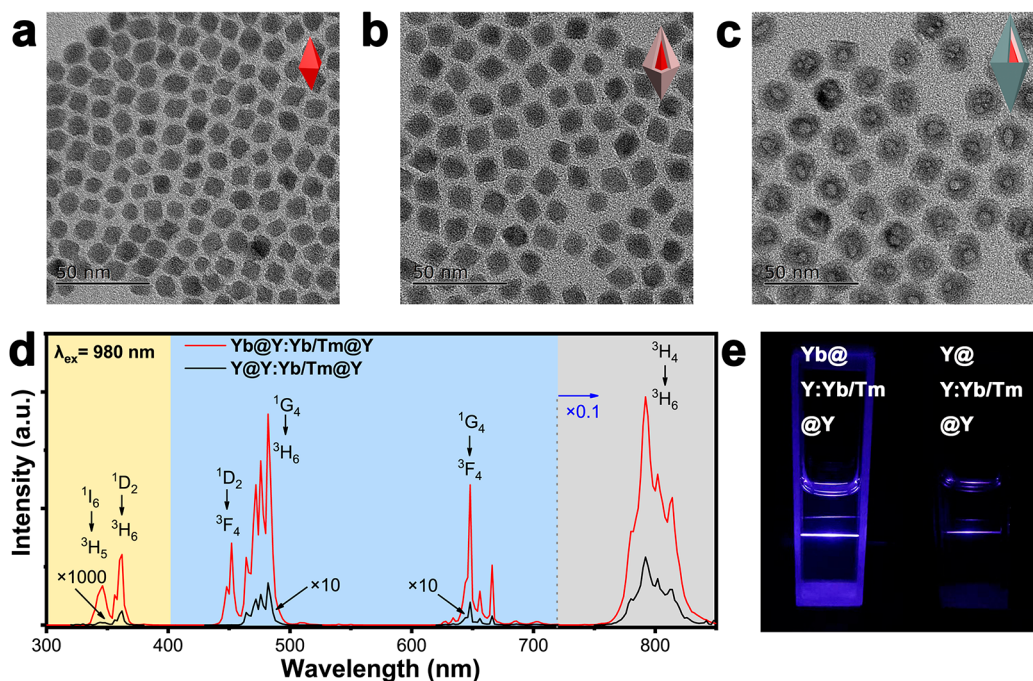
Figure 1. TEM images of as-synthesized (a) $LiYbF_4$ core, (b) Yb@Y:Yb/Tm(25%/0.5%) core@shell, and (c) Yb@Y:Yb/Tm(25%/0.5%)@Y core@shell@shell NPs, showing an increment in size for the core seeds with growing the interlayer and subsequent outermost shell layer. (d) Upconversion emission spectra for Yb@Y:Yb/Tm@Y and Y@Y:Yb/Tm@Y nanoparticles upon 980 nm excitation. (e) Luminescent photograph for Yb@Y:Yb/Tm@Y (left) and Y@Y:Yb/Tm@Y (right).

to improve UCL. Little attention has been paid so far to increasing UV/blue UCL through dopants' spatial distribution and concentration.

We proposed a host sensitization (Yb)-directed energy migration model in the $LiLnF_4$ host with the nanostructure of energy-absorbing active core@luminescent shell@inert shell. This host has low phonon energy and a high crystal field strength, which could not only improve high-order upconversion (i.e., UV/blue emission of Tm^{3+}), particularly with a higher UV emission ratio than the sodium hosts,[21] but also overcome the challenges of controlling the synthesis of smaller and uniform β-$NaYbF_4$.[22] The Yb^{3+}-rich core in this design could elevate the absorption cross-section of the NPs and provide more excitation energy to targeted emitters. Our results demonstrated that this nanostructure could provide considerably enhanced multiphoton upconversion luminescence compared to nanostructures reported so far, which are the following. (1) The well-recognized insulator system (Y@Y:Yb/Tm@Y) contains a relatively low level of Yb^{3+} dopants. (2) For the reverse structure (YbTm@Yb@Y), the Yb sensitized layer was located closer to the outside environment, easily resulting in the excited-state ET to the surface defects as unfavorably applied to FRET-based applications since the FRET efficiency is proportional to r^{-6} (r is the donor–acceptor distance).[23] (3) For the fully doped structure (YbTm@YbTm@Y, namely, traditional core@shell structure), the additional Tm^{3+} doped caused a nonnegligible energy loss for high-order UCL of Tm^{3+} due to breaking of the Yb^{3+}–Yb^{3+} energy migration and increasing of Tm^{3+}–Tm^{3+} cross-relaxation. This study adds to our knowledge of how active ions' spatial distribution and concentration affect UCL boosting. The obtained Yb-based UCNPs have a wide range of potential applications.

The $LiLnF_4$ nanocrystal was selected as the host to improve the multiphoton emission of Tm^{3+}, and the desired Yb@Y:Yb/Tm@Y NPs were synthesized via the previously reported epitaxial growth method.[24] The XRD patterns obtained from the as-obtained NPs (Figure S1a) show the tetragonal structure that matched the standard XRD cards ($LiYbF_4$ PDF no. 71-1211, $LiYF_4$ PDF no. 85-0806). The resulting NPs were diamond-shaped with uniform in size, as evidenced by TEM images (Figure 1) and size distribution histograms (Figure S1c). The size of Yb@Y:Yb/Tm@Y gradually increased from (10.52 ± 0.96) nm × (13.74 ± 1.21) nm ($LiYbF_4$ core) and (13.72 ± 1.07) nm × (16.60 ± 1.24) nm (core@shell) to (20.43 ± 1.49) nm × (24.20 ± 1.44) nm (core@shell@shell). EDX elemental mapping also confirmed its elemental composition (Figure S1b).

According to previous reports, the doping level of Tm^{3+} was set as 0.5% mol for acquiring bright UV/blue emission.[15] To compare the role of active core on the UCL, Y@Y:Yb/Tm@Y NPs (Yb^{3+}-free core) was synthesized. These NPs have particle size distributions and shell thicknesses similar to Yb@Y:Tm/Yb@Y NPs (Figure S2). However, there exists significant UCL enhancements in 346 nm ($^1I_6 \rightarrow {}^3H_5$), 362 nm ($^1D_2 \rightarrow {}^3H_6$), and 452 nm ($^1D_2 \rightarrow {}^3F_4$) emissions over 5000-fold as well as about 2 orders of magnitude amplification in other emission peaks (482 nm ($^1G_4 \rightarrow {}^3H_6$) and 648 nm ($^1G_4 \rightarrow {}^3F_4$)) (482 nm: 50.16), and their corresponding luminescent spectra and photographs are shown in Figure 1d and Figure 1e, respectively. The latter luminescence enhancement via intuitive contrast attributed to the inner sensitizing $LiYbF_4$ core amplifies the injected excitation energy, indicating that a stronger ET upconversion occurs in the codoped Y:Yb/Tm emitting layer.

We then examined the ET/migration dynamics to confirm the underlying mechanism in the enhancement. First, we
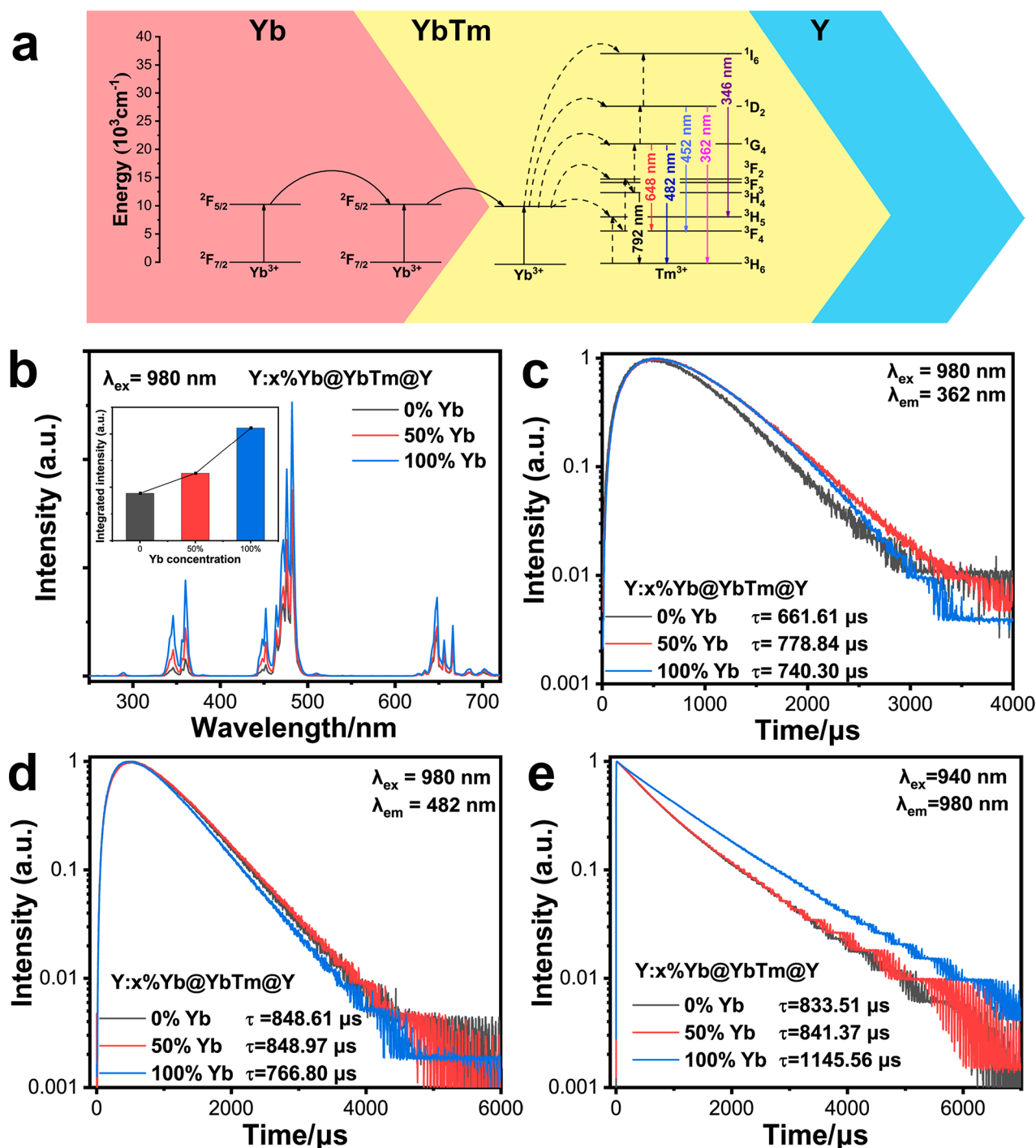
Figure 2. (a) Schematic illustration of the ET for Yb@YbTm@Y nanoparticles under 980 nm excitation. (b) UCL spectra of Y:x%Yb@YbTm@Y NPs under 980 nm excitation,. Inset: integrated UCL intensity of Y:x%Yb@YbTm@Y NPs. Decay curves of Y:x%Yb@YbTm@Y NPs under 980 nm excitation at (c) 362 nm and (d) 482 nm. (e) Decay curves of Y:x%Yb@YbTm@Y NPs under 940 nm excitation at 980 nm (x = 0, 50, 100).

investigated the effect of the Yb^{3+} ions concentration in the luminescent layer on its upconversion process. By comparison (Figure S3a), the inert shell passivation results in different multiples of enhancement between the determined Yb^{3+} content samples, and the UCL intensity of UCNPs decreased with increasing concentration of Yb^{3+} ions (25%, 50%, 99.5%) with a 3.5 nm thickness of $LiYF_4$ shell (Figure S3b). We speculated a considerable concentration quenching effect that confined the UCL intensity and efficiency. We further passivated the surface of UCNPs by thickening the inert

shell from 3.5 nm to 5.5 nm (Figure S3d). Thus, the UCL intensity increases dramatically, especially in Yb@Yb:0.5% Tm@Y NPs (Figure S3c), increasing over 2 orders of magnitude. It suggested that an inert epitaxial shell could overcome the concentration quenching of active Yb^{3+} ions by preventing excitation energy coupling to the surface defects. In addition, the quantum yield (QY) of Yb@Yb:0.5%Tm@Y NPs was determined to be 0.23% under 980 nm excitation at 0.4 W/cm^2, which is higher than that of $NaYF_4$:Yb,Tm (d = 20 nm, QY = 0.04%) NPs.
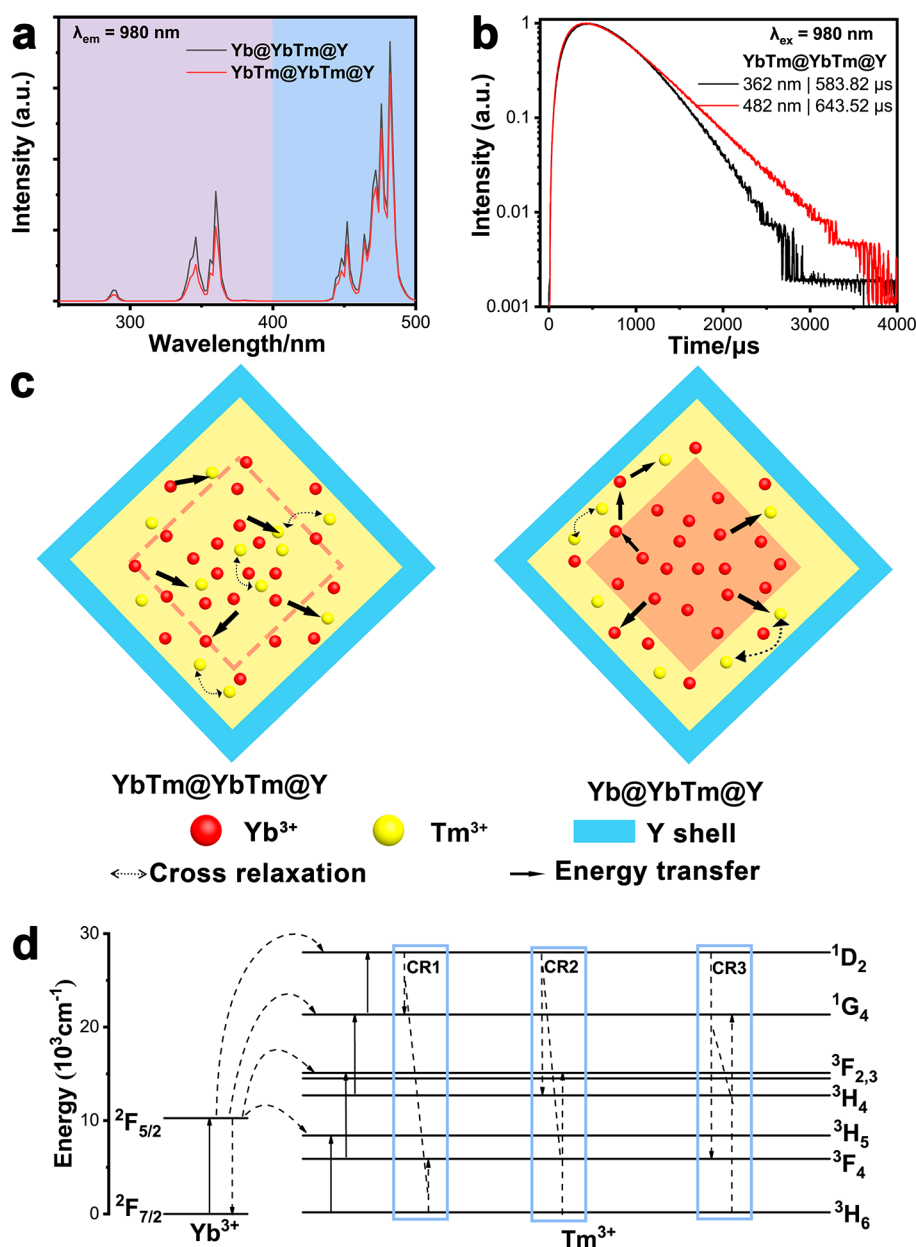
Figure 3. (a) UCL of Yb@YbTm@Y and YbTm@YbTm@Y NPs under 980 nm excitation. Decay curves of YbTm@YbTm@Y NPs under 980 nm excitation at (b) 362 and 482 nm. (c) Diagrams of YbTm@YbTm@Y and Yb@YbTm@Y NPs. (d) Proposed cross-relaxation mechanisms in YbTm@YbTm@Y nanoparticles under 980 nm excitation.

Additionally, we investigated the Tm^{3+} concentration in Yb/Tm "alloy" shell of Yb@Yb:x%Tm@Y NPs (x = 0.5, 1, 2). Compared to Yb:0.5%Tm NPs, the UCL intensities of the Yb:1%Tm and Yb:2%Tm NPs decreased due to the unwanted cross-relaxation (Figure S4). These findings suggested that the Yb:0.5%Tm had enormous potential to improve multiphoton UCL. Meanwhile, a set of Yb@Yb:0.5%Tm@Y (abbreviated as Yb@YbTm@Y) NPs with shell thickness ranging from 3, 5.5, and 6.5 to 7.5 nm was developed (Figure S5). Initially, we observed a steady increase in UCL with the brightest luminescence at 5.5 nm intermediate shell thickness, after which the luminescence intensity decreased. It indicates that the designed nanostructure can effectively suppress the consumption of excitation energy in a larger space through long-range $Yb^{3+}-Yb^{3+}$ energy migration attributed to the Yb core, whereas the reported Y@Yb:1%Tm@Y NPs with a 1−2

nm spatial confined energy migration.[25] It also demonstrates the advantages of a host-sensitized core in energy manipulation.

Furthermore, we optimized the doping level of Yb^{3+} in the core. Figure 2b shows that the Yb@YbTm@Y owned the strongest UCL under 980 nm excitation in the comparable size and morphology (Figures S1c, S2a, and S6). Compared to the Y@YbTm@Y, the UCL enhancement factors at 362 nm caused by 50% and 100% Yb concentrations were 2.8 and 5.7, and 1.26 and 1.86 enhancements at 482 nm, respectively. However, these enhancement factors were smaller than those of NPs with 25% Yb in the luminescent layer (Figure 1d) due to the decrease of the absorption ratio. To explore the reasons for UCL enhancement of Tm^{3+}, we first determined the contribution to luminescence from increased absorption (energy acquisition). According to the absorption spectra
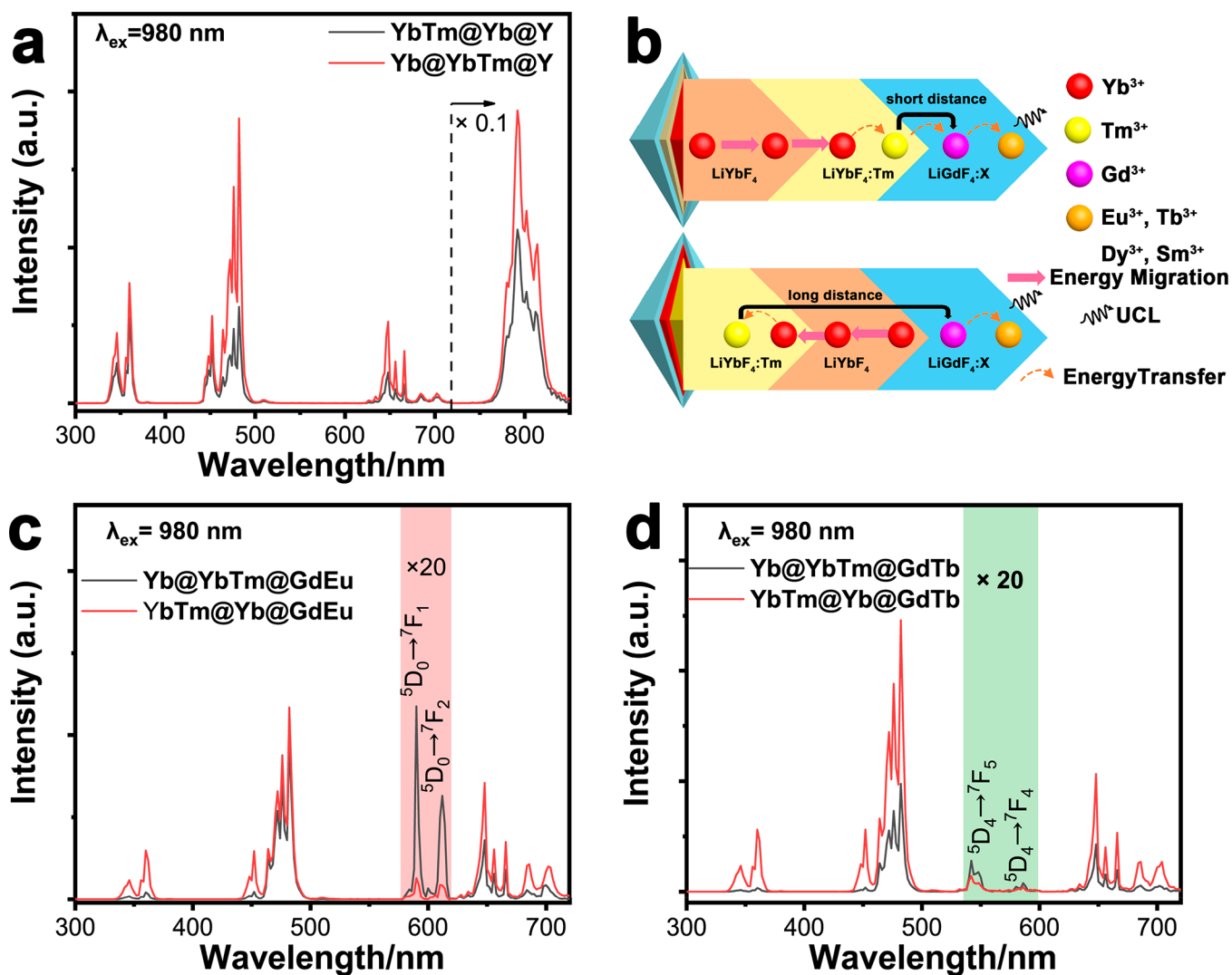
Figure 4. (a) UCL of Yb@YbTm@Y and YbTm@Yb@Y NPs under 980 nm excitation. (b) Illustration of the samples Yb@YbTm@GdEu (Tb, Dy, and Sm) and YbTm@Yb@ GdEu (Tb, Dy, and Sm) NPs and the energy transport processes. UCL of (c) Yb@YbTm@GdEu and YbTm@Yb@GdEu NPs and (d) Yb@YbTm@GdTb and YbTm@Yb@GdTb NPs under 980 nm excitation.

(Figure S7a), the Yb@YbTm@Y NPs could obtain 2-fold energy from the excitation source under the same conditions. Also, the enhancement factors are not equal to the absorption increase due to the nonlinear UCL process. Therefore, we measured the decay curves of multiphoton upconversion of Tm^{3+} under 980 nm excitation. Notably, the decay curve of the upconversion process was divided into two parts: the rise time and the decay time (Figure 2a). The decay time at 362 nm was first increased and then decreased with the increase of the Yb^{3+} content in the core (Figure 2c), but the rising time at 362 nm emission became longer with increased Yb^{3+} concentration (0% Yb, 499 μs; 50% Yb, 506 μs; 100% Yb, 552 μs). Notably, compared with Y@YbTm@Y NPs, the rise time of Yb@ YbTm@Y increased by 10.6%, implying that the $Yb^{3+}-Yb^{3+}$ energy migration would increase the energy population of Tm^{3+}. Then Tm^{3+} could obtain more energy through increased $Yb^{3+}-Yb^{3+}$ energy migration, thereby improving the UCL. However, the Y:50%Yb@YbTm@Y NPs had the longest rise (0% Yb, 503 μs; 50% Yb, 534 μs; 100% Yb, 525 μs) and decay (0% Yb, 848.61 μs; 50% Yb, 848.97 μs; 100% Yb, 794.72 μs) time for 482 nm emission (Figure 2d), demonstrating that the

ET process from Yb^{3+} in the core region to Tm^{3+} would affect the luminescent decay process of Tm^{3+}.

We also investigated the Yb^{3+} downshifting emission decay curve under 940 nm irradiation, which could explain why increasing the Yb^{3+} concentration would increase the energy population of Tm^{3+} UCL. Figure 2e shows that NPs with more Yb^{3+} owned a longer lifetime at 980 nm emission. The upconversion process will experience competition of positive and negative feedback as Yb^{3+} concentration rises. Besides, higher Yb^{3+} concentrations reduced the distance between adjacent ions, resulting in faster energy transport and a shorter lifetime. Conversely, the probability of energy migration between distant ions increased, lengthening the lifetime. The positive feedback in the internal sensitization layer exceeds the negative feedback for the $^1D_2$ population, but the $^1G_4$ population experienced a negative impact when the Yb^{3+} concentration increased from 50% to 100%.

In summary, an increase in internal Yb^{3+} ions enhances the ET probability to the activator via a long-range process, increasing the multiphoton population of Tm^{3+} ions and ultimately enhancing UCL. Also, the pump power dependence of Y:x%Yb@YbTm@Y supported this conclusion. Taking 362
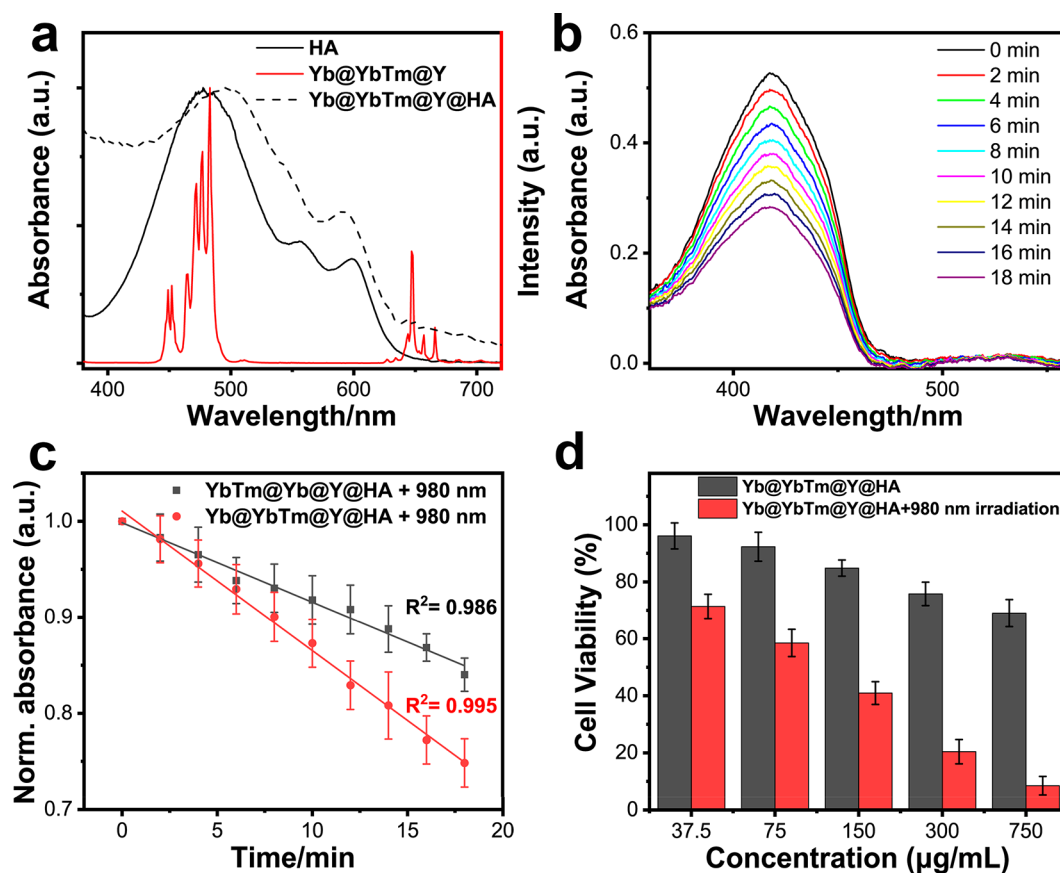
Figure 5. (a) Absorption spectrum of HA and Yb@YbTm@Y@HA overlap with the emission of Yb@YbTm@Y. (b) $^1O_2$ generation from Yb@YbTm@Y@HA was detected by monitoring DPBF absorbance with 980 nm laser irradiation time. (c) $^1O_2$ generation from YbTm@Yb@Y@HA and Yb@YbTm@Y@HA NPs detected by DPBF as a function of 980 nm laser irradiation time. (d) Cell viabilities of 4T1 cells under different concentrations of Yb@YbTm@Y@HA nanocomposites and treatment methods.

and 482 nm emissions as examples, the value of n became smaller with higher Yb^{3+} content (Figure S7b,c), and the differences of n at 362 nm are greater than those at 482 nm. Furthermore, compared with emission processes of 362 and 482 nm, the latter experienced more negative feedback, resulting in a slight decrease in the value of n. These results were also consistent with the present analysis, implying competition for negative and positive feedback brought by the increase in Yb^{3+} concentration, with the competition having different impacts on different energy levels.

We also extended the activator ions to Er^{3+}. Figure S8 shows that there is also an approximately 65-fold and 9-fold enhancement of Er^{3+} ions for 405 and 540 nm emission under 980 nm excitation (8.14 W/cm^2). Nevertheless, the enhanced factor is smaller than the high-level UCL emission of Tm^{3+} due to the 405 nm and 540 nm emissions being from a three- and two-photon upconversion process. Besides, we extended this structure to the NaLnF$_4$ host, and the NaYF$_4$ core was employed as the seed to prepare samples due to the uncontrollable of NaYbF$_4$. The Y@Yb@Y:Yb/Tm@Y NPs also showed much stronger UCL than Y@Y@Y:Yb/Tm@Y NPs, as depicted in Figure S9.

Moreover, we compared the Yb:0.5%Tm@YbTm@Y (shorten by YbTm@YbTm@Y) structure with Yb@YbTm@Y to test the increased activators, which could further enhance the UCL. Interestingly, our Yb@YbTm@Y NPs performed better in multiphoton UCL under 980 nm excitation (Figure 3a). Notably, the luminescent intensity at 362 nm is 1.47 times that

of YbTm@YbTm@Y, but the emission intensity at 800 nm is slightly weaker (Figure S10). Typically, more luminescent centers will result in higher luminescence intensity without concentration quenching effects. The luminescence dynamics of these two NPs were then investigated to reveal the critical mechanism responsible for anomalous emission. Not only did the YbTm@YbTm@Y have a shorter rise time (362 nm, 476 μs; 482 nm, 455 μs), but it also owned a shorter decay time (362 nm, 583.82 μs; 482 nm, 643.52 μs) (Figure 3b and Figure S11c,d). It was proposed that Tm^{3+} doped in the core region caused additional depopulation processes of its high-lying energy level due to $Tm^{3+}-Tm^{3+}$ cross-relaxation (Figure 3c). Moreover, increasing Tm^{3+} concentration will enhance the cross-relaxation among Tm^{3+} ions,[26,27] leading to a shorter decay time. According to the energy matching principle, several possible cross-relaxation pathways related to the $^1D_2$ state are proposed (Figure 3d). These processes include CR1: $^1D_2 \rightarrow {}^3F_4$: $^3H_6 \rightarrow {}^1G_4$, CR2: $^1D_2 \rightarrow {}^3H_4$: $^3H_6 \rightarrow {}^3F_2$, CR3: $^1D_2 \rightarrow {}^1G_4$: $^3H_6 \rightarrow {}^3F_4$, decreasing the lifetime of 362 nm emission. Furthermore, we synthesized Tm^{3+}-free NPs with a similar nanostructure (Yb@Yb@Y) to compare the downshifting process under 940 nm excitation to investigate the ET between Yb^{3+} and Tm^{3+}. As a result of Tm^{3+} in specific spatial regions, the decay time gradually decreased from 1861.78 μs to 1145.56 μs to 941.57 μs (Figure S11a). It demonstrated that when the Tm^{3+} is codoped with Yb^{3+} in the core region, the excitation energy harvested by Yb^{3+} ions preferentially transfers the excitation energy to adjacent Tm^{3+} ions instead of energy

transport from core to luminescent layer, resulting in a shorter rise time. Namely, the long-range $Yb^{3+}-Yb^{3+}$ migration was broken by $Yb^{3+}-Tm^{3+}$ energy transfer in core region of YbTmYbTm@Y NPs. These findings demonstrated that the spatial distribution of the activators played a significant role in energy transport. The excitation energy transition from Yb^{3+} to Tm^{3+} required a longer path in Yb@YbTm@Y NPs than in YbTm@YbTm@Y, and the $Tm^{3+}-Tm^{3+}$ cross-relaxation was reduced, resulting in a longer decay time and more efficient high-order UCL.

The traditional sensitization structure has recently been modified to be a nanostructure with the sensitizer on the outer layer and the activator on the inner layer.[17,28,29] Compared to the traditional sensitization structure, the activator in the outer layer is closer to the energy acceptor outside, making energy transfer easier, thus improving the utilization rate of high-order UCL. When the luminescence of the forward (Yb-core) and reverse (YbTm-core) structures was compared, the forward-structured NPs exhibit brighter UCL from 300 to 850 nm (Figure 4a). And then, we measured the decay time of the Yb@YbTm@Y and YbTm@Yb@Y for UCL at 362 and 482 nm and found that the rising and decay time was shorter for the latter NPs (Figure S12a,b). Overall, such a design (Yb@YbTm@Y NPs) minimizes the injected energy leakage due to surface quenching, allowing more pump energy to be transferred to higher Tm^{3+} excited states and thus increasing its multiphoton UCL. To highlight the benefits of our designed NPs, we developed a $Tm^{3+} \rightarrow Gd^{3+} \rightarrow A^{3+}(Eu^{3+}/Tb^{3+})$ ET model by coating Gd^{3+} and A^{3+} ions on the surfaces of two oppositely structured NPs (Figure 4b). As an acceptor, Gd^{3+} could absorb the energy from Tm^{3+}, while A^{3+} ions were employed as probes, and the luminescence intensity was used to characterize the amount of transferred energy from Tm^{3+} to Gd^{3+}.

The presence of $Tm^{3+} \rightarrow Gd^{3+} \rightarrow Eu^{3+}$ ET was demonstrated by the characteristic peak of Eu^{3+} at 590 and 612 nm (Figure 4c). The integrated luminescence intensity of Eu^{3+} (580−620 nm) in the Yb@YbTm@Gd:15% Eu (shortened by Yb@YbTm@GdEu) sample is 6 times that of YbTm@Yb@GdEu. The UCL intensities of these samples quantified the ET efficiencies from Tm^{3+} to outside acceptors at 346 nm ($^1I_6 \rightarrow ^3H_5$) (normalized at 792 nm), 24.14% for Yb@YbTm@Y, and 0.85% for YbTm@Yb@Y NPs, suggesting that the ET was enhanced when the Tm^{3+} ions were placed in the outer layer. Consequently, the Eu^{3+} gained more energy to produce a stronger luminescence than YbTm@Yb@GdEu NPs. The comparison between Yb@YbTm@Gd:15%Tb (2% Sm, 2% Dy) (shortened by Yb@YbTm@GdTb (Dy, Sm)) and YbTm@Yb@GdTb (Sm, Dy) NPs also supported this conclusion (Figure 4d and Figure S13a,b). These results demonstrated that the active core@shell@shell structured NPs owned a stronger UCL and performed better in ET-based applications.

To show the practical potential of the structure, we further tested its FRET-based application using photodynamic therapy (PDT) as a proof-of-concept expriment. As photosensitizers, hypocrellin A (HA) was loaded into the matrix of UCNPs-based micelles. The overlapping spectra and absorption spectra of Yb@YbTm@Y@HA shown in Figure 5a confirmed the successful preparation of nanophothosensitizer, indicating a suitable FRET couple. Next, 1,3-diphenylisobenzofuran (DPBF) was employed as a probe to assess the ability of Yb@YbTm@Y@HA composites to produce $^1O_2$ (Figure 5b).

As a result, the Yb@YbTm@Y@HA composite shows a higher $^1O_2$ generation rate (Figure 5c), demonstrating better ET capability. The methylthiazolyldiphenyltetrazolium bromide (MTT) assay was used to assess the PDT effects on 4T1 cells (Figure 5d). We found that the cell viability at 75 μg/mL is 58%, indicating the potential of PDT for cancer therapy.

In summary, we used a nanostructure design to investigate the effect of spatial distribution and concentration of the sensitizer Yb^{3+} on the UCL of Tm^{3+}. Compared to commonly used sensitizers in the outer layer, the Yb host-sensitized core reduces injected energy leakage caused by surface quenching, allowing pump photons to accumulate energy at higher Tm^{3+} excited states to boost UCL or efficiently transfer the energy to the acceptor. The present results show that our Yb host-sensitized core@luminescent shell@inert shell nanostructure achieves the highest efficiency of multiphoton UCL of Tm^{3+} activators to date, opening up new channels for manipulating the energy interactions to fulfill various applications requiring bright UV/blue emission.

■ ASSOCIATED CONTENT

Ⓢ Supporting Information

The Supporting Information is available free of charge at https://pubs.acs.org/doi/10.1021/acs.nanolett.2c01324.

> Experimental section, characterization methods, XRD spectra, element mapping, size distribution histograms of samples, fluorescence spectra, pump power dependence of UCL, and comparison of UCL lifetimes for different samples (PDF)

■ AUTHOR INFORMATION

Corresponding Author

Yulei Chang − *State Key Laboratory of Luminescence and Applications, Changchun Institute of Optics, Fine Mechanics and Physics, Chinese Academy of Sciences, Changchun 130033 Jilin, China;* ⓞ orcid.org/0000-0001-7223-1797; Email: yuleichang@ciomp.ac.cn

Authors

Xiaoyu Xie − *State Key Laboratory of Luminescence and Applications, Changchun Institute of Optics, Fine Mechanics and Physics, Chinese Academy of Sciences, Changchun 130033 Jilin, China; University of the Chinese Academy of Sciences, Beijing 100049, China*

Qiqing Li − *State Key Laboratory of Luminescence and Applications, Changchun Institute of Optics, Fine Mechanics and Physics, Chinese Academy of Sciences, Changchun 130033 Jilin, China*

Haoran Chen − *State Key Laboratory of Luminescence and Applications, Changchun Institute of Optics, Fine Mechanics and Physics, Chinese Academy of Sciences, Changchun 130033 Jilin, China; University of the Chinese Academy of Sciences, Beijing 100049, China*

Wang Wang − *State Key Laboratory of Luminescence and Applications, Changchun Institute of Optics, Fine Mechanics and Physics, Chinese Academy of Sciences, Changchun 130033 Jilin, China; University of the Chinese Academy of Sciences, Beijing 100049, China*

Fengxia Wu − *State Key Laboratory of Luminescence and Applications, Changchun Institute of Optics, Fine Mechanics and Physics, Chinese Academy of Sciences, Changchun 130033 Jilin, China; Institute of Molecular Medicine, College*

of Life and Health Sciences, Northeastern University, Shenyang 110819 Liaoning, China

Langping Tu − *State Key Laboratory of Luminescence and Applications, Changchun Institute of Optics, Fine Mechanics and Physics, Chinese Academy of Sciences, Changchun 130033 Jilin, China*

Youlin Zhang − *State Key Laboratory of Luminescence and Applications, Changchun Institute of Optics, Fine Mechanics and Physics, Chinese Academy of Sciences, Changchun 130033 Jilin, China*

Xianggui Kong − *State Key Laboratory of Luminescence and Applications, Changchun Institute of Optics, Fine Mechanics and Physics, Chinese Academy of Sciences, Changchun 130033 Jilin, China*

Complete contact information is available at:
https://pubs.acs.org/10.1021/acs.nanolett.2c01324

Author Contributions

Y.C. conceived the experiments. X.X., H.C., W.W., and F.W. performed the experiments. X.X., Q.L., L.T., and Y.C. analyzed the data and prepared the manuscript. Y.Z. and X.K. gave suggestions on the experiments. All authors contributed to manuscript writing and discussions.

Notes

The authors declare no competing financial interest.

■ REFERENCES

(1) Chatterjee, D. K.; Rufaihah, A. J.; Zhang, Y. Upconversion fluorescence imaging of cells and small animals using lanthanide doped nanocrystals. *Biomaterials* **2008**, *29*, 937−943.

(2) Chen, G. Y.; Qiu, H. L.; Prasad, P. N.; Chen, X. Y. Upconversion Nanoparticles: Design, Nanochemistry, and Applications in Theranostics. *Chem. Rev.* **2014**, *114*, 5161−5214.

(3) Yang, D.; Ma, P. a.; Hou, Z.; Cheng, Z.; Li, C.; Lin, J. Current advances in lanthanide ion (Ln^{3+})-based upconversion nanomaterials for drug delivery. *Chem. Soc. Rev.* **2015**, *44*, 1416−1448.

(4) Wang, D.; Liu, B.; Quan, Z.; Li, C.; Hou, Z.; Xing, B.; Lin, J. New advances on the marrying of UCNPs and photothermal agents for imaging-guided diagnosis and the therapy of tumors. *J. Mater. Chem. B* **2017**, *5*, 2209−2230.

(5) Qin, W. P.; Zhang, D. S.; Zhao, D.; Wang, L. L.; Zheng, K. Z. Near-infrared photocatalysis based on YF_3: Yb^{3+}, Tm^{3+}/TiO_2 core/shell nanoparticles. *Chem. Commun.* **2010**, *46*, 2304−2306.

(6) Liu, S.; Huang, J.; Yan, L.; Song, N.; Zhang, P.; He, J.; Zhou, B. Multiphoton ultraviolet upconversion through selectively controllable energy transfer in confined sensitizing sublattices towards improved solar photocatalysis. *J. Mater. Chem. A* **2021**, *9*, 4007−4017.

(7) Richards, B. S.; Hudry, D.; Busko, D.; Turshatov, A.; Howard, I. A. Photon Upconversion for Photovoltaics and Photocatalysis: A Critical Review. *Chem. Rev.* **2021**, *121*, 9165−9195.

(8) Fischer, S.; Siefe, C.; Swearer, D. F.; McLellan, C. A.; Alivisatos, A. P.; Dionne, J. A. Bright Infrared-to-Ultraviolet/Visible Upconversion in Small Alkaline Earth-Based Nanoparticles with Biocompatible CaF_2 Shells. *Angew. Chem., Int. Ed.* **2020**, *59*, 21603−21612.

(9) Hirsh, D. A.; Johnson, N. J. J.; van Veggel, F. C. J. M.; Schurko, R. W. Local Structure of Rare-Earth Fluorides in Bulk and Core/Shell Nanocrystalline Materials. *Chem. Mater.* **2015**, *27*, 6495−6507.

(10) Fischer, S.; Bronstein, N. D.; Swabeck, J. K.; Chan, E. M.; Alivisatos, A. P. Precise Tuning of Surface Quenching for Luminescence Enhancement in Core−Shell Lanthanide-Doped Nanocrystals. *Nano Lett.* **2016**, *16*, 7241−7247.

(11) Wang, L.; Li, Y. Controlled Synthesis and Luminescence of Lanthanide Doped NaYF4 Nanocrystals. *Chem. Mater.* **2007**, *19*, 727−734.

(12) Zuo, J.; Li, Q. Q.; Xue, B.; Li, C. X.; Chang, Y. L.; Zhang, Y. L.; Liu, X. M.; Tu, L. P.; Zhang, H.; Kong, X. G. Employing shells to eliminate concentration quenching in photonic upconversion nanostructure. *Nanoscale* **2017**, *9*, 7941−7946.

(13) Yan, L.; Zhou, B.; Song, N.; Liu, X.; Huang, J.; Wang, T.; Tao, L.; Zhang, Q. Self-sensitization induced upconversion of Er^{3+} in core−shell nanoparticles. *Nanoscale* **2018**, *10*, 17949−17957.

(14) Chen, B.; Kong, W.; Wang, N.; Zhu, G. Y.; Wang, F. Oleylamine-Mediated Synthesis of Small $NaYbF_4$ Nanoparticles with Tunable Size. *Chem. Mater.* **2019**, *31*, 4779−4786.

(15) Zuo, J.; Tu, L. P.; Li, Q. Q.; Feng, Y. S.; Que, I.; Zhang, Y. L.; Liu, X. M.; Xue, B.; Cruz, L. J.; Chang, Y. L.; et al. Near Infrared Light Sensitive Ultraviolet-Blue Nanophotoswitch for Imaging-Guided "Off-On" Therapy. *ACS. Nano.* **2018**, *12*, 3217−3225.

(16) Zhou, B.; Huang, J. S.; Yan, L.; Liu, X. L.; Song, N.; Tao, L. L.; Zhang, Q. Y. Probing Energy Migration through Precise Control of Interfacial Energy Transfer in Nanostructure. *Adv. Mater.* **2019**, *31*, 1806308.

(17) Zhou, B.; Yan, L.; Huang, J.; Liu, X.; Tao, L.; Zhang, Q. NIR II-responsive photon upconversion through energy migration in an ytterbium sublattice. *Nat. Photonics.* **2020**, *14*, 760−766.

(18) Song, N.; Zhou, B.; Yan, L.; Huang, J. S.; Zhang, Q. Y. Understanding the Role of Yb^{3+} in the Nd/Yb Coupled 808-nm-Responsive Upconversion. *Front. Chem.* **2019**, *6*, 673.

(19) Chen, B.; Wang, F. Emerging Frontiers of Upconversion Nanoparticles. *Trends. Chem.* **2020**, *2*, 427−439.

(20) Liang, Y.; Zhu, Z.; Qiao, S.; Guo, X.; Pu, R.; Tang, H.; Liu, H.; Dong, H.; Peng, T.; Sun, L.-D.; et al. Migrating photon avalanche in different emitters at the nanoscale enables 46th-order optical nonlinearity. *Nat. Nanotechnol.* **2022**, *17*, 524−530.

(21) Mahalingam, V.; Vetrone, F.; Naccache, R.; Speghini, A.; Capobianco, J. A. Colloidal Tm^{3+}/Yb^{3+}-Doped $LiYF_4$ Nanocrystals: Multiple Luminescence Spanning the UV to NIR Regions via Low-Energy Excitation. *Adv. Mater.* **2009**, *21*, 4025−4028.

(22) Chen, B.; Wang, F. Recent advances in the synthesis and application of Yb-based fluoride upconversion nanoparticles. *Inorg. Chem. Front.* **2020**, *7*, 1067−1081.

(23) Jares-Erijman, E. A.; Jovin, T. M. FRET imaging. *Nat. Biotechnol.* **2003**, *21*, 1387−1395.

(24) Li, X. M.; Shen, D. K.; Yang, J. P.; Yao, C.; Che, R. C.; Zhang, F.; Zhao, D. Y. Successive Layer-by-Layer Strategy for Multi-Shell Epitaxial Growth: Shell Thickness and Doping Position Dependence in Upconverting Optical Properties. *Chem. Mater.* **2013**, *25*, 106−112.

(25) Chen, X.; Jin, L.; Kong, W.; Sun, T.; Zhang, W.; Liu, X.; Fan, J.; Yu, S. F.; Wang, F. Confining energy migration in upconversion nanoparticles towards deep ultraviolet lasing. *Nat. Commun.* **2016**, *7*, 10304−10309.

(26) Wei, W.; Zhang, Y.; Chen, R.; Goggi, J.; Ren, N.; Huang, L.; Bhakoo, K. K.; Sun, H.; Tan, T. T. Y. Cross Relaxation Induced Pure Red Upconversion in Activator- and Sensitizer-Rich Lanthanide Nanoparticles. *Chem. Mater.* **2014**, *26*, 5183−5186.

(27) Yadav, R.; Singh, S. K.; Verma, R. K.; Rai, S. B. Observation of multi-mode: Upconversion, downshifting and quantum-cutting emission in Tm^{3+}/Yb^{3+} co-doped Y_2O_3 phosphor. *Chem. Phys. Lett.* **2014**, *599*, 122−126.

(28) Zhou, B.; Tang, B.; Zhang, C.; Qin, C.; Gu, Z.; Ma, Y.; Zhai, T.; Yao, J. Enhancing multiphoton upconversion through interfacial energy transfer in multilayered nanoparticles. *Nat. Commun.* **2020**, *11* (1), 1174.

(29) Joshi, R.; Perala, R. S.; Shelar, S. B.; Ballal, A.; Singh, B. P.; Ningthoujam, R. S. Super Bright Red Upconversion in $NaErF_4$:0.5% Tm@$NaYF_4$:20%Yb Nanoparticles for Anti-counterfeit and Bioimaging Applications. *ACS Appl. Mater. Interfaces* **2021**, *13*, 3481−3490.

📖 **Recommended by ACS**

Remarkably Enhanced Red Upconversion Emission in β-$NaLuF_4$:Er,Tm Microcrystals via Ion Exchange

Xiaolong Chen, Jing Feng, *et al.*

JULY 06, 2022
INORGANIC CHEMISTRY
READ 🗗

Investigation of the Energy Loss in Upconversion Luminescence of Lanthanide-Doped Nanocrystals for Anticounterfeiting and a Nanoheater

Yanqing Hu, Qiyue Shao, *et al.*

OCTOBER 19, 2022
ACS APPLIED NANO MATERIALS
READ 🗗

Enhancement of Upconversion Luminescence by the Construction of a 3Yb-Er-Hf Sublattice Energy Cluster and Surface Defect Elimination

Han Yu, Qingming Huang, *et al.*

MARCH 21, 2022
INORGANIC CHEMISTRY
READ 🗗

Uranium-Sensitized Luminescence Enhancement in $Li_2B_4O_7$:U^{6+},Eu^{3+} and Potential Application towards Color-Tunable Phosphors and Actinide Sensor

Reshmi T. P., Santosh K. Gupta, *et al.*

SEPTEMBER 15, 2022
ACS APPLIED OPTICAL MATERIALS
READ 🗗

Get More Suggestions >